Amaia Morales, Fabio Hernández-Ramos, Leyre Sillero, Rut Fernández-Marín, Izaskun Dávila, Patricia Gullón, Xabier Erdocia, Jalel Labidi, Multiproduct biorefinery based on almond shells: impact of the delignification stage on the manufacture of valuable products, Bioresource Technology, Volume 315, 2020, Article number 123896, Online ISSN: 1873-2976, https://doi.org/10.1016/j.biortech.2020.123896.

(https://www.sciencedirect.com/science/article/pii/S0960852420311688?via%3Dihub)

Abstract: In this work, an integral valorisation of almond shells through a biorefinery approach was studied. The three main components of almond shells were extracted, isolated and characterised. The autohydrolysis process permitted the extraction of the hemicellulosic fraction obtaining a liquor rich in xylooligosaccharides (22.12 g/L). Then, two different delignification processes, alkaline and organosolv treatments, were proposed to obtain a very high purity lignin (≈90%) which could be further valorised for a wide variety of applications. The valorisation of the high cellulosic content of the delignified solids was carried out using two different methods. On the one hand, producing cellulose nanocrystals and on the other hand obtaining glucose by an enzymatic hydrolysis as well as a spent solid mainly composed by lignin (≈78 wt.%). Thus, the proposed biorefinery approach could contribute to a circular economy as all the main components of the almond shells could be revalorised by environmentally friendly procedures.

Keywords: Biorefinery, lignin, cellulose, hemicellulosic oligosaccharides, nanocrystals, almond shells

Multiproduct biorefinery based on almond shells: impact of the delignification stage on the manufacture of valuable products

Amaia Morales[1], Fabio Hernández-Ramos[1], Leyre Sillero[1], Rut Fernández-Marín[1], Izaskun Dávila[1], Patricia Gullón[1], Xabier Erdocia[2], Jalel Labidi[1*]

[1]Chemical and Environmental Engineering Department. University of the Basque Country UPV/EHU. Plaza Europa, 1, 20018 San Sebastian (Spain)
[2]Department of Applied Mathematics. University of the Basque Country UPV/EHU. Rafael Moreno "Pichichi", 3, 48013 Bilbao (Spain)
*Corresponding author. jalel.labidi@ehu.es

Abstract

In this work, an integral valorisation of almond shells through a biorefinery approach was studied. The three main components of almond shells were extracted, isolated and characterised. The autohydrolysis process permitted the extraction of the hemicellulosic fraction obtaining a liquor rich in xylooligosaccharides (22.12 g/L). Then, two different delignification processes, alkaline and organosolv treatments, were proposed to obtain a very high purity lignin (≈90%) which could be further valorised for a wide variety of applications. The valorisation of the high cellulosic content of the delignified solids was carried out using two different methods. On the one hand, producing cellulose nanocrystals and on the other hand obtaining glucose by an enzymatic hydrolysis as well as a spent solid mainly composed by lignin (≈78 wt.%). Thus, the proposed biorefinery approach could contribute to a circular economy as all the main components of the almond shells could be revalorised by environmentally friendly procedures.

Keywords: Biorefinery, lignin, cellulose, hemicellulosic oligosaccharides, nanocrystals, almond shells

1 Introduction

The depletion of fossil resources, in addition to its contribution to the global environmental crisis, makes it necessary to look for alternatives for the not too distant future. Utilisation of renewable resources, such as agricultural crops and associated residues, forestry residues, marine biomass resources, industrial side streams and food supply chain side streams would be necessary in the transition to a green and circular economy (Ioannidou et al., 2020).

In this new global scenario, biorefineries are called to play a significant role. The concept of biorefinery is considered to be one of the pillars of research in recent years and the best option for transforming different biomass systems into high added-value products such as biofuels and chemicals (Dragone et al., 2020). However, it is important to define exactly the type of biomass to be used, since it needs to be an available, abundant and low-cost raw material in order to make the process economically profitable. In this context, in the last decades, lignocellulosic biomass, which is mainly composed by cellulose, hemicelluloses and lignin, has been outlined as a viable alternative. In order to valorise these three major fractions of the biomass in a biorefiney facility, several pretreatments have been studied. On the one hand, autohydrolysis is a pretreatment applied to lignocellulosic materials which employs only water as solvent at subcritical conditions (150–230 °C and 4.9–20 bars) to disrupt the lignocellulosic structure and facilitate the subsequent processes for biomass valorisation. In the autohydrolysis pretreatment the water is auto-ionized into H_3O^+ and OH^- and act as catalyst dissolving and depolymerizing the hemicellulosic fraction (Ruiz et al., 2020). On the other hand, in delignification treatments, lignin is isolated from the lignocellulosic biomass. Among the most studied and more environmentally friendly processes that can be used in a biorefinery, alkaline and organosolv treatments stand out. In the first one, a wide range of temperatures can be employed (25-150 ºC) along with different alkali agents, such as, NaOH and KOH that cause swelling of biomass and the removal of the lignin compounds by saponification of intermolecular ester bonds and alteration of the lignin structure. Otherwise, in organosolv treatments lignin is extracted from lignocellulosic feedstock by lignin dissolution

using organic solvents (ethanol, methanol, etc.) or aqueous solutions of them. These treatments can be carried out in a wide range of temperature (100-250 °C) and normally under high pressures.

Within the biorefinery context, several works have been carried out based on different lignocellulosic materials to valorise their major fractions. Regarding to the hemicelluloses, this component can be used to obtain different products such as xylooligosaccharides (Dávila et al., 2019; B. Gullón et al., 2018) or furfural (Zang et al., 2020). Otherwise, lignin can be employed as a precursor of many products in a wide range of application fields (Fernández-Rodríguez et al., 2017). Finally, cellulose, the Earth's main natural renewable polymer, has a wide range of possibilities in industry. It can be converted into glucose for further transformation into bioethanol (Ko et al., 2020), but it can also be used to obtain cellulose nanocrystals which can be employed in many areas such as, biological medicine, food packaging, photoelectric materials and other fields (Wang et al., 2020).

In 2018, world almond trees cultivation represented around 2.1 million cultivated hectares, of which around 660,000 corresponded to Spain (FAOSTAT statistical database, 2018) The cultivation of almond trees generates between 70 and 150 million tons of almond shells annually (de Hoyos-Martínez et al., 2018) and, as no industrial/commercial application of them has been still recognized, they are usually burned to obtain energy or dumped into landfill without any control which can cause environmental problems (Kaur et al., 2020). Therefore, in order to valorise this lignocellulosic residue and thus promote the circular economy while minimizing the environmental issues regarded to its current management, it was chosen as the feedstock for the biorefinery approach proposed in this work. In line with the purpose of this work, in the latest years, some new applications are being studied in order to revalorise this residue. For instance, several authors (Ko et al., 2020; Nitsos et al., 2018) have studied the production of bioethanol or the obtaining of cellulose nanocrystals (Khili et al., 2019).

Taking the above ideas into account, the aim of this work was to develop a multiproduct biorefinery in cascade based on almond shells through their integral valorisation fitted to the circular economy model. The proposed sequence would allow the obtaining of multiple products

with potential applications both as platform chemicals and building blocks. To accomplish this objective, the almond shells were subjected to a first stage of autohydrolysis obtaining an oligosaccharide rich liquid phase and a cellulose and lignin rich solid phase. This solid was fractionated applying organosolv and alkaline delignification treatments to study their effects on the chemical structure of both resulting lignin and cellulose pulp. These pulps were bleached and used for the production of cellulose nanocrystals. Finally, the pulps from the two delignification treatments as well as the both bleached solids were subjected to an enzymatic hydrolysis to produce glucose. Thus, the influence of the delignification treatments and of the bleaching stage on the feasibility of the enzymatic saccharification of the solids to yield glucose was analysed. All obtained fractions were isolated, weighed and deeply characterised employing different analytical techniques. The scheme that has been followed is the one shown in the Figure 1.

Therefore, this work provides a whole biorefinery scheme for the integral revalorization of the almond shells taking into account all the components of this lignocellulosic material. Therefore, green and circular economy is boosted by giving an economic value to these residues making them a source of prebiotic oligosaccharides, added-value aromatic compounds and glucose or cellulose nanocrystals.

2 Materials and methods

2.1 Raw material

Local farmers supplied the almond shells (AS), variety Marcona. Once collected, AS were dried at room temperature until constant moisture and then they were milled and sieved to obtain a homogenised lot with a particle size smaller than 4 mm, which was stored in a dry and dark place and further employed in the different treatments.

2.2 Autohydrolysis treatment

The autohydrolysis conditions of AS were the same than the reported by Nabarlatz et al. (2005). Shortly, the treatment was performed in a 1.5 L stainless steel 5100 Parr reactor with a 4848 Parr controller operating in isothermal regime at 179 ºC for 23 minutes, with a liquid/solid ratio (LSR)

of 8 (g/g in oven-dried basis). Once the reaction time was over, the reactor was cooled down and the solid and liquid phases were separated by filtration. The solid phase was washed with water and it was stored at 4 ºC until use, while the liquid phase or autohydrolysis liquor, which contained the solubilised products from the hemicellulosic fraction, was characterised.

In order to be able to compare the results obtained with other works the severity of the autohydrolysis treatment was measured by the combination of the temperature and the reaction-time of the isothermal treatment. The calculation of the Severity factor (S_0) considering the heating, maintenance and cooling periods was done as previously reported (Aguilar et al., 2018).

2.3 Delignification treatments

The solid from the autohydrolysis stage of almond shells (AAS) was subjected to two different delignification processes. On the one hand, an organosolv process was performed using a dissolution of 70/30 EtOH/water (v/v) at 200 °C and 90 min with constant stirring and a LSR of 6 (mL/g) (Fernández-Rodríguez et al., 2017) in a 1.5 L stainless steel 5100 Parr reactor. On the other hand, an alkaline treatment employing a sodium hydroxide solution (7.5 wt.%), at 121 °C for 90 min and using a LSR of 6 (mL/g) (Fernández-Rodríguez et al., 2017) in an autoclave using borosilicate glass bottles was carried out.

After the delignification processes, the suspensions were filtered and the recovered solid fractions were washed with water until neutral pH, they were air-dried and stored until use. On the other hand, the lignin contained in the black liquors was precipitated by adding two volumes of acidified water (pH 2) in the case of organosolv liquors (de Hoyos-Martínez et al., 2018) and by acidification with H_2SO_4 until pH 2 in the case of alkaline liquors (Dávila et al., 2017).

2.4 Bleaching of the delignified solids

The solids obtained by organosolv (O-DS) and alkaline (A-DS) delignifications were bleached. This process was carried out with acetic acid, sodium hypochlorite and distilled water following the method described by Wise et al. (1946) with slight modifications. The bleaching treatment was performed at 75 ºC in an oil bath under constant stirring during 2 h. After that time, the solid

and liquid fractions were separated by vacuum filtration. Then, the solid fractions were washed with distilled water until neutral pH. Finally, these solid fractions or pulps (O-BP and A-BP) were dried at 50 ºC for 24 h.

2.5 Cellulose nanocrystal (CNC) obtaining

Organosolv and alkaline cellulose nanocrystals (O-CNC and A-CNC) were obtained from the bleached pulps (O-DS and A-DS) by an acid hydrolysis following a modified method reported by Barbosa et al. (2016). This step was performed with 33 wt.% H_2SO_4 (ratio 1/15 g/mL, CNC: H_2SO_4) at 60 ºC for 1 h in an ultrasound bath. After the acid hydrolysis, distilled water was added to the suspension to stop the reaction. Then, the CNC and liquid fraction were separated by vacuum filtration and the CNC were washed with distilled water to remove the excess of H_2SO_4 until neutral pH. Finally, distilled water was added to nanocrystals and they were sonicated to keep the suspension stable.

2.6 Enzymatic hydrolysis of the delignified and bleached AS

The enzymatic hydrolysis of the delignified (O-DS and A-DS) and bleached (O-BP and A-BP) AS was carried out in Erlenmeyer flasks with an orbital agitation of 150 rpm at 48.5 °C. The pH of the samples was kept at 4.85 using a 0.05 N citric acid-sodium citrate buffer and using a LSR of 16 (g/g in oven-dried basis). The enzymatic cocktail used in an enzyme to solid ratio (ESR) of 20 FPU/g. The hydrolysis was lasted up to 72 h and at given reaction times samples were withdrawn from the reaction media, centrifuged, filtered, diluted and analysed by HPLC for the quantification of monosaccharides following the method described by Dávila et al. (2017).

At the end of the enzymatic hydrolysis, the liquid and solid phases were separated by filtration. The solid phase was washed with water for several times and it was chemically characterised.

2.7 General characterisation

The methods followed for the chemical characterisation of the raw material, the analysis of the solids obtained after different treatments, the chemical characterisation of the liquid phase from autohydrolysis treatment and the extracted lignins are displayed in Table 1.

3 Results and discussion

3.1 Raw material composition

The chemical composition of the AS used in this work was 3.1 wt.% of ash, 3.7 wt.% of extractives, 29.7 wt.% of insoluble lignin, 16.7 wt.% of glucan and 31.6 wt.% of hemicelluloses (measured as the joint contribution of xylan, arabinosyl substituents and acetyl groups). In molar ratio, the composition of the hemicelluloses was xylose:arabinose:acetyl groups 10:0.3:4.4. These results were in agreement with the results reported by de Hoyos-Martinez et al. (2018).

3.2 Autohydrolysis treatment

Based on the chemical composition of AS, it was considered feasible to use this raw material to obtain oligosaccharides derived from its hemicelluloses. For this, an autohydrolysis treatment was carried out in order to perform a selective extraction of the hemicellulosic fraction, resulting in a liquor rich in oligosaccharides (Davila et al., 2016). The removal of the hemicelluloses from this feedstock and its conversion into oligosaccharides could permit the revalorization of this fraction due to the prebiotic and antioxidant activity of these compounds (P. Gullón et al., 2018).

During the autohydrolysis of the AS (S_0: 3.87), 40.3 wt.% of the initial raw material was solubilised. The solubilisation observed in this work for the AS was higher than the one reported by Nabarlatz et al. (2005) for this feedstock subjected to an autohydrolysis under the same conditions (33.6 wt.%).

The solubilisation of the AS was attributed to the hemicellulosic fraction, thus, an autohydrolysis liquor rich in oligomeric and monomeric carbohydrates and degradation products was obtained. The autohydrolysis process obtained a solubilisation of more than 80% of the hemicellulosic fraction; however, this treatment also solubilised about 24% of the lignin content (Table 2), since hydrothermal processes results in a hydrolysis of hemicelluloses and some lignin degradation

(Huang et al., 2019b). Among the obtained oligosaccharides, the xylooligosaccharides (XOS) were the most abundant ones (22.12 g/L). 61.4% of the xylan was converted into XOS, which is a higher percentage than the one reported by B. Gullón et al. (2018) for chestnut shells (56%). An important cleavage of the arabinosyl substituents of the xylan was also appreciated as 27.0% of them were released as arabinose. This is due to their high susceptibility to the autohydrolysis treatments as it was previously reported by Dávila et al. (2016). Due to the low glucan conversion during the autohydrolysis (2.8%), it could be supposed that the majority of the glucan determined in the AS presented a cellulosic origin, as only amorphous cellulose is solubilised in hot water (Sixta et al., 2006).

Hemicelluloses are biopolymers present in lignocellulosic materials that act as connectors between cellulose and lignin, so after their elimination the solid that remains is rich in cellulose and lignin, and it is ready for the next valorisation step following the biorefinery approach. In addition, during extraction, the porosity of the feedstock is expected to increase since certain amount of mass is removed leaving the solid more accessible for the next stage (Cocero et al., 2018). Thus, this would make the subsequent delignification stage more efficient. Table 2 shows the chemical composition of AAS.

3.3 Delignification treatments

As the chemicals, the operational conditions and, hence, the mechanisms of delignification involved in each process (organosolv or alkaline) were different, the solid and lignin yields achieved for each case were expected to vary (Fernández-Rodriguez et al., 2017). After the organosolv treatment, the recovered solid accounted almost a 66%, while for the alkaline treatment this recovery was slightly higher (≈69%). Moreover, the delignifications were successfully carried out since the observed lignin loss during the treatments was high. The alkaline delignification leaded to a 37.12% of lignin removal, whereas the organosolv delignification permitted around 35.09% of lignin solubilisation, yielding solids with a 34.66% and a 38.41% of this fraction, respectively. A similar behaviour was reported by other authors after subjecting AAS to these two types of delignification processes (Fernández-Rodríguez et al., 2017). A 2.39%

of the glucan fraction was removed during the organosolv treatment, while this fraction was not affected by the alkaline one, resulting in delignified solids with a 46.32% and a 50.38% of glucan, respectively. The hemicellulosic fraction still present after the previous autohydrolysis treatment was affected by the delignifications. Indeed, both treatments leaded to the solubilisation of the hemicellulosic fraction, but the removal during the alkaline treatment was slightly higher (59.77%) than during the organosolv one (40.11%).

After gravimetrically quantifying the amount of lignin precipitated after each delignification, the percentage of the recovered lignin with respect to the initial lignin amount in the sample was calculated. For the organosolv delignification, the recovered lignin amount was around 34.60%, whereas for the alkaline delignification this percentage was around 46.66%. These results are in agreement with the obtained lignin withdrawal. Moreover, regarding the eliminated lignin amount during the delignifications, both precipitations showed high recovery yields (≈100%).

3.4 Bleaching of the delignified solids

The delignified solids obtained during the organosolv and alkaline treatments were subjected to a bleaching process prior to the obtaining of cellulose nanocrystals or to subjecting them to an enzymatic hydrolysis. After the bleaching, solids mainly composed by cellulose were achieved, as it could be seen in Table 2 for the O-BP and the A-BP, since the lignin has been almost completely removed independently of the process used during the delignification. The effectivity of the sodium hypochlorite used during the bleaching process to remove the lignin fraction was due to its ability to oxidize, brighten and solubilise lignin (Abu-Thabit et al., 2020). The removal of the lignin from the delignified solids was also reflected by an increase of the crystallinity index (CI) of the bleached pulps compared with the CI observed for the delignified solids (CI % = 58.11% for O-DS, 65.11% for A-DS, 67.41% for O-BP and 69.78% for A-BP). According to Karimi and Taherzadeh (2016) the increase in the crystallinity index could be associated to the removal of amorphous regions of the lignocellulosic biomass such as lignin, hemicelluloses, proteins or pectins and not only the amorphous cellulose.

3.5 Enzymatic hydrolysis of the delignified and bleached solids

In order to study the effect of the delignification procedure used to remove the lignin from AAS on a subsequent enzymatic hydrolysis, O-DS and A-DS were hydrolysed using the enzymatic cocktail Cellic Ctek 2. The bleached pulps (O-BP and A-BP) were also subjected to the same enzymatic hydrolysis, in order to evaluate if the almost complete removal of the lignin achieved during the bleaching exerted an important benefit on the subsequent enzymatic hydrolysis.

The enzymatic susceptibility of the different solids was analysed by determining the glucan to glucose conversion (GnGC). This parameter considers the ratio between the glucose released during the enzymatic hydrolysis and the potential glucose present in the solid, which could be achieved by the total conversion of the glucan present in the solid. The calculation of the GnGC was carried out using the following equation (Eq 1), where the value 1.11 refers to the conversion factor of glucan to glucose (Huang et al., 2019a).

$$GnGC\ (\%) = \frac{Glucose\ in\ enzymatic\ hydrolysate\ (g)}{Initial\ glucan\ in\ substrate\ (g) \cdot 1.11} \cdot 100 \qquad (Eq.1)$$

Figure 2 shows the glucan to glucose conversion of the different solids and it could be appreciated that, independently of the treatment to which the AS were subjected, the conversion in all the cases was close to 100%. Similar GnGC was achieved by Morales et al. (2018) when they carried out the enzymatic hydrolysis of chestnut shells after subjecting them to an alkaline delignification using the Cellic Ctek 2 cocktail.

Although all the solids presented a very high susceptibility towards the enzymatic hydrolysis as with all of them a conversion of almost 100% of the glucan contained in the solids was achieved, the bleached pulps produced a higher quantity of glucose. The concentration of glucose achieved at the end of the enzymatic hydrolysis when the bleached pulps were used was 43.5 g/L for O-BP and 49.1 g/L for A-BP solid, while the concentration of glucose when the not-bleached solids were used was 34.0 g/L for O-DS and 35.6 g/L for A-DS. This is associated to the higher cellulosic content of the O-BP and A-BP, since they were mainly composed by cellulose as it was shown in Table 2. The higher glucose production with bleached pulps was also observed by Costa et al.

(2018) when they studied the enzymatic hydrolysis of banana rachis delignified by different procedures. They observed that the enzymatic hydrolysis of the banana rachis subjected to an oxidative treatment with sodium hypochlorite leaded to a production of 44.7% (w/w) of glucose, while the banana rachis subjected to an organosolv treatment with ethanol leaded to a production of 19.8% (w/w) of glucose.

It could be expected that the bleached pulps would present a higher GnGC due to their higher crystallinity index (see section 3.4) and their lower lignin content as it could be seen in Table 2. Commonly solids with low lignin content are more susceptible towards an enzymatic hydrolysis, as lignin on the one hand could block the approach of the enzymes to the cellulose and it could also bind irreversibly to the enzyme through hydrophobic interactions, decreasing its activity (Hu et al. 2013). However, the GnGC achieved with the non-bleached solids was higher than the one obtained with the bleached pulps, as it can be seen in Figure 2. This could be explained, on the one hand, because the lignin content of the solids only affected the enzymatic hydrolysis up to some extent. Zhu et al. (2008) observed that when the lignin content of hybrid polar mixed with sparse wood chips decreased from 24.5% to 14.8% the digestibility of the solid increased, but when the lignin content of the solids was below 14.8% the susceptibility of the solids towards the enzymatic hydrolysis did not increase. On the other hand, the lower crystallinity index of the cellulose present in the delignified AS was also a benefit for the enzymatic hydrolysis as the crystalline cellulose is more recalcitrant than the amorphous cellulose. Due to the disordered structure of the amorphous cellulose, the enzymes access and hydrolyse it easier.

Thus, the two delignification procedures employed on the autohydrolysed AS produced solids with a higher susceptibility towards the production of glucose than the bleached solids. Among the delignified solids, the organosolv ones presented a higher GnGC due to their lower crystallinity. The employment of these solids for the production of glucose permitted the obtaining of a spent solid mainly composed by lignin, as it can be seen in the Table 2, which could be further revalorised. It has been reported that the lignins extracted from ethanol residues obtained by a simultaneous enzymatic hydrolysis and saccharification presented a higher

reactivity for the production of polyurethanes or epoxy resins than the lignosulphonate or Kraft lignins (Qiao et al., 2016).

3.6 Characterisation of the isolated fractions

3.6.1 Characterisation of the solids

3.6.1.1 ATR-FTIR

The AS presented the typical bands corresponding to a lignocellulosic structure (Urruzola et al., 2014). The spectrum of AAS was quite different to the spectrum of AS. The band around 3350 cm^{-1}, together with the ones in the range from 2840 to 2945 cm^{-1}, got substantially intensified. These bands were related to the stretching vibrations of -OH and -CH groups, which mainly form part of the cellulose and lignin structures (Ahorsu et al., 2019; Chen et al., 2015; Kasiri and Fathi, 2018; Urruzola et al., 2014). Another great variation was observed for the band at around 1610 cm^{-1}, which corresponded to the O-H bending of the adsorbed water in carbohydrates (Kasiri and Fathi, 2018; Urruzola et al., 2014). The band that appeared more notably around 1424 cm^{-1} after the autohydrolysis treatment represented -CH_2 scissor motion in cellulose and confirmed the removal of the hemicellulosic fraction (Tan et al., 2019). Although no significant changes were observed on the bands detected at 1740 cm^{-1} and 1375 cm^{-1} also attributed to hemicelluloses, the high intensification of the band at 1510 cm^{-1} related to the aromatic skeletal vibration of lignin suggested that the hemicellulosic fraction was eliminated and lignin component became more abundant on the solid (Ahorsu et al., 2019).

The solids obtained after the delignification treatments (O-DS and A-DS) presented similar ATR-FTIR spectra to the one presented by AAS but with some changes. The main variations were again observed on the bands in the range from 2840 to 2945 cm^{-1}. Nevertheless, the maintenance of these bands suggests that the cellulose component of AS was not removed during delignification treatments (Xiao et al., 2019). The variation on the intensity of the characteristic peaks of cellulose could mean a possible degradation during the treatments (Tan et al., 2019). The reduction of the intensity of the bands around 1510 and 1230 cm^{-1}, attributed to the C-C aromatic skeletal vibration and =C-O-C axial asymmetric strain, indicated the elimination of lignin and

hemicelluloses (Xiao et al., 2019). This was also appreciated on the disappearance of the broad band at 1730 cm^{-1} after the alkaline delignification but not after the organosolv one. This decrease indicated the possible cleavage of hemicelluloses-lignin association (Tan et al., 2019).

The intensification of some bands in the samples organosolv and alkaline post enzymatic hydrolysis solid (O-HES and A-HES) such as the ones at 1602, 1510 and 1423 cm^{-1}, attributed to aromatic ring vibration, indicated that the aromatic ring structures were more present (Xu et al., 2020). The peaks corresponding to C-O vibrations in syringyl and guaiacyl groups at 1330 and 1264 cm^{-1}, respectively, also strengthened (Xu et al., 2020). This demonstrates that the solid got enriched in lignin as cellulose was converted into glucose due to the enzymatic hydrolysis (Dávila et al., 2017).

As for O-BP and A-BP, both samples presented an important intensification of the band around 3350 cm^{-1}, coupled with a slight shift to a lower wavenumber. The bands between 2840 and 2945 cm^{-1} became a single band in the case of O-BP, and for A-BP the bands remained as small shoulders. A clear disappearance of the lignin-assigned peak at 1510 cm^{-1} was observed especially in O-BP, suggesting complete lignin removal through the bleaching step (Xiao et al., 2019). The increase of the band at 1160 cm^{-1} was attributed to C-O glycosidic bond asymmetrical stretching present in cellulose. The growth of the intense band at 1030 cm^{-1}, which was attributed to the C-O-C pyranose ring stretching vibration, meant that the solid was enriched in cellulose (Kasiri and Fathi, 2018; Xiao et al., 2019). The band around 1435 cm^{-1} indicated the presence of crystalline cellulose, while the band at 898 cm^{-1} corresponded to the amorphous cellulosic part (Orue et al., 2019; Tan et al., 2019).

Comparing the ATR-FTIR spectra of O-BP, A-BP, O-CNC and A-CNC, it was observed that all spectra were similar, which demonstrates that there were no changes in the chemical structure of cellulose during the hydrolysis treatment. O-CNC and A-CNC samples showed two important peaks around 3335 and 2896 cm^{-1}, just like O-BP and A-BP, corresponding to the O-H stretching vibration and symmetric C-H vibration, respectively. The peak around 1317 cm^{-1} was attributed to O-H bending, while peaks at 1160 and 1030 cm^{-1} for glycosidic bonds and pyranose ring

vibrations, respectively, were also remarkable in O-CNC and A-CNC. (Thakur et al., 2020; Xiao et al., 2019).

3.6.1.2 X-Ray Diffraction (XRD)

In order to analyse the effect of different treatments on the crystalline structure of the solids, XRD analyses were carried out. Crystals consist on planes of atoms that are separated and ordered in a certain manner (Kasiri and Fathi, 2018). Cellulose has a crystalline structure due to the hydrogen bonds and Van der Waals forces between its adjacent molecules. On the other hand, hemicelluloses and lignin present an amorphous structure (Kasiri and Fathi, 2018).

The diffractograms of the different solids presented the characteristic peaks at around 16.2°, 22.4°, and 34.7°, which were attributed to the (110), (002), and (004) crystallographic planes, respectively (Xiao et al., 2019), which corresponded to the crystallographic domains of cellulose (Kasiri and Fathi, 2018; Xiao et al., 2019). Nevertheless, it was observed that the intensity at the main crystalline peak (22.4º) increased as the raw material was subjected to the different treatments. In other words, after the autohydrolysis had been done, the intensity of the peak increased and it was also narrower, meaning that the solid had a greater crystallinity degree, and confirming the hemicellulosic fraction removal (Kasiri and Fathi, 2018). As a consequence of the alkaline delignification, the intensity of same peak underwent a significant growth, thus confirming the lignin elimination. However, organosolv delignification did not have such a big impact on the crystallinity of the solid, since the diffractograms of AAS and O-DS were similar.

As expected for O-HES and A-HES, the XRD patterns clearly showed a reduction on crystallinity, as enzymes attack cellulose microfibrils (Dávila et al., 2017), which are the only components of biomass with high crystallinity degree. In both solids, the enzymatic hydrolysis lead to an almost complete disappearance of the peaks at 16.2° and 34.7º, and the one at 22.4° got significantly reduced.

After the bleaching stage, the peak at 22.4º of A-BP presented an almost identical diffractogram as the one after delignification, whereas O-BP presented a meaningful raise.

In the diffraction patterns of O-BP, A-BP, O-CNC and A-CNC chiefly three crystalline diffractions were discerned from 15 to 35º at 2θ. The samples presented the (110), (002) and (004) planes which, as abovementioned, corresponded with the diffraction patterns of cellulose-I structure around 16.5˚, 22.8˚ and 35˚, respectively (Thakur et al., 2020; Xiao et al., 2019).

The crystallinity index (CI %) of O-BP, A-BP, O-CNC and A-CNC was calculated. In both treatments (organosolv and alkaline), cellulose nanocrystals (CI % O-CNC: 68.53% and A-CNC: 71.66%) presented a higher CI % comparing with the bleached pulps (CI % O-BP: 67.41% and A-BP: 69.78%). This is due to the removal of the amorphous part during the acid hydrolysis. These results are in accordance with other works in which CI % values of CNC between 54 and 88% were obtained (Thakur et al., 2020).

3.6.1.3 Thermogravimetric Analysis (TGA)

Thermogravimetric analyses of the solids were carried out in order to study the influence of the treatments on their thermal stability. The obtained TGA and DTG curves are shown in Figure 3. It is known that lignocellulosic biomass is characterised by several degradation steps (Xiao et al., 2019) and the solids before and after the delignification stage presented three steps. The first weight loss below 100 ºC, presented by all the analysed samples, corresponded to water evaporation, while the second and main degradation step between 200 and 400 ºC was attributed to degradation of structural components of the biomass including the depolymerisation, dehydration and decomposition of glycosidic units (Xiao et al., 2019). Finally, the third weight loss was observed above 400 ºC, which corresponded to the oxidation and breakdown of charred residue into low molecular weight gaseous components (Xiao et al., 2019).

For the AS, four degradation steps were detected: the first one corresponding to sample humidity (≈70 ºC), one at 290 ºC probably corresponding to the early degradation of hemicelluloses, lignin and other non-cellulosic components (Kasiri and Fathi, 2018), the main degradation step at 350 ºC and the last around 430 ºC and till the end of the test. This thermogram was in accordance with

that obtained by Urruzola et al., (2014). The residue left by the degradation of AS accounted a 23% of the initial weight.

The notable weight loss at 290 ºC in AS disappeared for AAS, probably due to the elimination of the hemicellulosic fraction. The main degradation step shifted to a higher temperature (370 ºC). Orue et al. (2019) and Kasiri and Fathi (2018) also detected a similar behaviour on their samples and they ascribed this thermal stability enhancement to the removal of hemicelluloses. Moreover, the accounted final residue for this solid was of around 20% of its initial weight.

It was seen that A-DS had its maximum degradation temperature at 341 ºC, while organosolv lignin (O-L) had it main degradation at 352 ºC. This second stage was attributed principally to the thermal degradation of the main component of AS, cellulose, and also to the lignin and hemicelluloses still remaining in the solid (Orue et al., 2019). The diminution on the main degradation temperature could have been observed due to a possible prior degradation during the delignification process. Orue et al. (2019) also reported similar results for their alkaline-treated walnut shells, relating them to the degradation of the cellulose chains of the sample suffered during the alkaline treatment. After the third degradation step, the residues left by O-DS and A-DS solids were 19.3% and 26.5% of the initial weight, respectively. This difference could be attributed to the fact that the chemicals employed in alkaline processes tend to leave inorganic impurities in the solid, whereas the organic solvents employed for organosolv extractions do not (Fernández-Rodríguez et al., 2017).

O-HES and A-HES still presented the three degradation steps abovementioned for the rest of the solids. Nevertheless, the main degradation step shifted to higher temperatures (360 and 345 ºC for O-HES and A-HES, respectively) probably due to the enrichment in lignin achieved after the glucan being converted into glucose (Dávila et al., 2017). There was no change on the third degradation step except for the residues left by O-HES and A-HES, which accounted 33.5% and 29.2% of the initial weight, respectively. This augment on the left residue could be attributed to the content in recalcitrant carbohydrates, proteins, and salts acquired during the enzymatic hydrolysis (Nitsos et al., 2016).

After the bleaching step, the main degradation temperatures showed a slight increase. For O-BP, this temperature raised to 357 ºC whereas for A-BP it grew to 356 ºC. This might be ascribed to the purification effect of the bleaching process, similarly to what had previously reported for their chemically-purified cellulose fibres (Urruzola et al., 2014). Both bleached solids left a 10% of their initial weight as final residue.

O-CNC and A-CNC demonstrated 3 similar degradation steps. In the second step, the highest mass loss was observed between 300 and 360 ºC and it was due to cellulose degradation. These results are aligned with the ones reported by other authors (Kamelnia et al., 2019; Xiao et al., 2019). However, the maximum degradation temperatures for O-CNC and A-CNC (302 and 316 ºC, respectively) were lower than the ones reported for O-BP and A-BP, which could be due to the fact that hydrolysis treatment with sulphuric acid causes the decrease in thermal stability (Xiao et al., 2019). The last degradation step was observed around 400 ºC and was attributed to cellulose pyrolysis (Kamelnia et al., 2019). The final residue obtained for O-CNC was around 13% and for A-CNC was 15% of their initial weight.

3.6.1.4 Characterisation of the nanocrystals by Atomic Force Microscopy (AFM)

The two bleached pulps (O-BP and A-BP) were subjected to acid hydrolysis, as previously described, in order to obtain CNC (O-CNC and A-CNC). After the obtained slurries were filtered, a dispersion of the CNC was prepared. The morphological properties and dimensions of the obtained nanocrystals (O-CNC and A-CNC) were determined by AFM, as it is shown in Figure 4. The nanocrystals exhibited sharp contours and a typically rod-like structure. O-CNC were slightly shorter in length than A-CNC (average 773.80 ± 77.03 nm and 860.09 ± 38.64 nm, respectively), whereas the width of O-CNC was higher than in A-CNC (average 70.05 ± 7.18 and 61.01 ± 5.37 nm, respectively). Similar results were reported by Mujtaba et al. (2017), who demonstrated greater diameters than 50 nm in cellulose nanocrystals obtained from flax fibres. Regarding the length of nanocrystals, the results obtained were in accordance with the results

obtained by Lizundia et al. (2020), who appreciated that the length of the nanocrystals could vary between 150 and 2000 nm depending on their origin.

3.6.2 Characterisation of the lignins

3.6.2.1 Purity

The purity of the lignins was analysed by quantitative acid hydrolysis in order to study the selectivity of each delignification treatment and, hence, to determine the amount of impurities such as hemicelluloses that had precipitated together with lignin under acidic medium. After the quantitative acid hydrolysis, the purities measured for the two obtained lignins were 88.76% for the organoslv lignin (O-L) and 89.76% for the alkaline lignin (A-L). These values were considerably high and they were in accordance with the ones reported for organosolv AS lignin (de Hoyos-Martínez et al., 2018; Fernández-Rodríguez et al., 2017) for A-L extracted from AS (Fernández-Rodríguez et al., 2017). Despite A-L being slightly purer, the amount of sugars coming from the hemicellulosic fraction in this sample (0.97%) was higher than the total sugar content in O-L (0.08%). This could be due to the selectivity of the organosolv process on lignin extraction, having less interaction with sugars (Fernández-Rodríguez et al., 2017).

3.6.2.2 Thermogravimetric Analysis (TGA)

The thermal stability of both lignins was determined by TGA. Figure 5 shows the thermograms of both lignins (O-L and A-L) and it could be appreciated that they presented similar behaviour in the whole temperature range. They mainly presented three degradation steps, where the first one was the dehydration stage, the second one was the active pyrolysis stage, and the last one the passive pyrolysis stage (Liu et al., 2016). The first stage took place at higher temperatures in the A-L (≈95 ºC) than in O-L (≈45 ºC) and there was a weight loss of around 3% due to water evaporation. The main degradation step happened at the same temperature in both lignins (≈365 ºC), which was in accordance with the values reported by other authors (Chen et al., 2015; de Hoyos-Martínez et al., 2018; Liu et al., 2016). This stage resulted into a weight loss of a 47% for A-L and 57% for O-L. It should be highlighted that A-L presented a shoulder at around 300 ºC,

which could be related to other impurities such as sugars. O-L did not present this shoulder, probably due to its lower sugars content. The last degradation step happened from 430 ºC on, and it leaded to a char formation of 36% in the case of O-L and 40% on A-L. These results were in accordance with the ones reported in the literature (de Hoyos-Martínez et al., 2018; Liu et al., 2016).

3.6.2.3 Total Phenolic Content (TPC)

The extraction method influenced the total phenolic content of lignin. The determined percentage of Equivalent Gallic Acid (% EGA) was 29.64% for O-L and 34.01% for A-L, which was 296.41 and 340.13 mg EGA/g lignin for O-L and A-L, subsequently. These values are in the range of the ones reported by Sequeiros et al. (2014); though they reported a higher number of EGA for O-L than for A-L. However, this difference could be related to the extraction conditions i.e. time, solvent concentrations and temperature (Dávila et al., 2017).

3.6.2.4 Molecular Weight

The molecular weight distributions of O-L and A-L leaded to the determination of their number-average (Mn), and weigh average (Mw) molecular weights as well as to their polydispersity indexes (Mw/Mn). The Mn for O-L and A-L were 1,555 and 1,615 Da, respectively, the Mw were 6,997 and 23,182 Da, subsequently. Therefore, the estimated Mw/Mn values were 4.50 and 14.35 for O-L and A-L, respectively. It should be noted that the equipment in which the analyses were carried out was calibrated with polystyrene standards. It was observed that lignins obtained through the different delignification processes (O-L and A-L) were substantially different in terms of molecular weight distribution. A-L presented higher Mw than O-L. This difference could be explained by several reasons. On the one hand, the conditions used in the delignification reactions had a big influence on the molecular weight distribution, decreasing the value of molecular weight as reaction conditions were harsher (Zhang et al., 2010). On the other hand, in alkaline medium, repolymerisation reactions occur, leading to an increase in the molecular weight of lignin (Morales et al., 2018). In addition, as mentioned above, A-L contained more impurities than O-L, resulting in an increase in molecular weight (Morales et al., 2018). Regarding polydispersity

index, it could be noted that A-L presented a higher heterogeneity. This could be explained due to the degradation of high molecular weight lignin molecules during the alkaline delignification process (Sun et al., 2012).

3.6.2.5 Lignin Composition and chemical structure (Py-GC/MS and ATR-FTIR)

A Py-GC/MS analysis was carried out to determine the composition of O-L and A-L using a pyrolysis temperature of 600 ºC to maximise the yield of the phenolic compounds (de Hoyos-Martínez et al., 2018) which are relevant in the valorisation of lignin. The compounds present in the O-L and A-L with an area greater than 1% are shown in Table 3. However, it was decided to also consider furfural in this list of compounds as, although its area was less than 1%, it provided relevant information about lignin. Furfural, is originated from the pyrolysis of carbohydrates that remain as impurities in lignin and was only present in A-L. This confirms what was mentioned above about the purity of lignins and provides another possible explanation for the difference in molecular weight between them (Morales et al., 2018).

Although compounds derived from fatty acids were also found, as detailed in Table 3, phenolic monomers represented 71-74% of the total compounds that were obtained. These phenolic compounds were classified into four groups as described by different authors based on their chemical structure and main formation pathways during thermal degradation (Chen et al., 2015; de Hoyos-Martínez et al., 2018; Fernández-Rodríguez et al., 2020; Ma et al., 2016), phenol-type compounds (P), guaiacol-type compounds (G), syringol-type compounds (S) and catechol-type compounds. However, in this case the catechol-type compounds were included in category (S) as they were degradation products of syringol during pyrolysis (Ma et al., 2016). Taking in to account the list of compounds reported in table 3, no significant differences between the two lignins were observed. In both cases, the chemical structure was mainly formed by guaiacol units and syringol units, 28-29% and 41-46% respectively, resulting in an S/G ratio of 1.45 for O-L and 1.56 for A-L, as shown in Table 3.

In addition, to verify that the chemical structure of the lignins was similar, an ATR-FTIR analysis was carried out and the two lignins showed the same characteristic peaks. It was therefore concluded, as abovementioned, that there were no changes in the chemical structure regardless of the extraction method that was used.

4 Conclusions

In this work, a complete biorefinery process for almond shells was proposed and validated. Firstly, oligosaccharides were obtained by autohydrolysis treatment. Secondly, lignin and cellulose rich solids were generated. Moreover, the latest were employed for glucose and nanocrystal production. The integral valorisation of such abundant waste would contribute to circular economy and zero-waste objective, increasing at the same time the economic value of this residue. According to the obtained results, it was concluded that depending on the selected process and the desired applications, products with different features could be obtained.

Acknowledgements

Authors want to acknowledge the University of the Basque Country UPV/EHU, as well as the Department of Economic Development and Infrastructure of the Spanish Government (CTQ2016-78689-R) for supporting financially this research. L.S. and R.F. would like to acknowledge the Department of Economic Development and Infrastructures of the Basque Government (scholarship of young researchers training). A.M. would like to thank the University of the Basque Country (Training of Researcher Staff, PIF17/207). The authors also want to acknowledge SGIker services from the University of the Basque Country UPV/EHU for their kind help with SEM, XRD and AFM analyses.

Supplementary data

Supplementary data associated with this work can be found in the online version of this paper where further characterisation of the solids and lignins are presented.

References

1. Abu-Thabit, N.Y., Judeh, A.A., Hakeem, A.S., Ul-Hamid, A., Umar, Y., Ahmad, A., 2020. Isolation and Characterization of Microcrystalline Cellulose from Date Seeds (Phoenix dactylifera L.). Int. J. Biol. Macromol. 155, 730–739. https://doi.org/10.1016/j.ijbiomac.2020.03.255
2. Aguilar, D.L., Rodríguez-Jasso, R.M., Zanuso, E., de Rodríguez, D.J., Amaya-Delgado, L., Sanchez, A., Ruiz, H.A., 2018. Scale-up and evaluation of hydrothermal pretreatment in isothermal and non-isothermal regimen for bioethanol production using agave bagasse. Bioresour. Technol. 263, 112–119. https://doi.org/10.1016/j.biortech.2018.04.100
3. Ahorsu, R., Cintorrino, G., Medina, F., Constantí, M., 2019. Microwave processes: A viable technology for obtaining xylose from walnut shell to produce lactic acid by Bacillus coagulans. J. Clean. Prod. 231, 1171–1181. https://doi.org/10.1016/j.jclepro.2019.05.289
4. Barbosa, A.M., Robles, E., Ribeiro, J.S., Lund, R.G., Carreño, N.L.V., Labidi, J., 2016. Cellulose nanocrystal membranes as excipients for drug delivery systems. Materials (Basel). 9, 1–15. https://doi.org/10.3390/ma9121002
5. Chen, L., Wang, X., Yang, H., Lu, Q., Li, D., Yang, Q., Chen, H., 2015. Study on pyrolysis behaviors of non-woody lignins with TG-FTIR and Py-GC/MS. J. Anal. Appl. Pyrolysis 113, 499–507. https://doi.org/10.1016/j.jaap.2015.03.018
6. Cocero, M.J., Cabeza, Á., Abad, N., Adamovic, T., Vaquerizo, L., Martínez, C.M., Pazo-Cepeda, M.V., 2018. Understanding biomass fractionation in subcritical & supercritical water. J. Supercrit. Fluids 133, 550–565. https://doi.org/10.1016/j.supflu.2017.08.012
7. Costa, S., Rugiero, I., Uria, C.L., Pedrini, P., Tamburini, E., 2018. Lignin degradation efficiency of chemical pre-treatments on banana rachis destined to bioethanol production. Biomolecules 8, 141. https://doi.org/10.3390/biom8040141
8. Dávila, I., Gordobil, O., Labidi, J., Gullón, P., 2016. Assessment of suitability of vine shoots for hemicellulosic oligosaccharides production through aqueous processing. Bioresour. Technol. 211, 636–644. https://doi.org/10.1016/j.biortech.2016.03.153
9. Dávila, I., Gullón, B., Alonso, J.L., Labidi, J., Gullón, P., 2019. Vine shoots as new source for the manufacture of prebiotic oligosaccharides. Carbohydr. Polym. 207, 34–43. https://doi.org/10.1016/j.carbpol.2018.11.065
10. Dávila, I., Gullón, P., Andrés, M.A., Labidi, J., 2017. Coproduction of lignin and glucose from vine shoots by eco-friendly strategies: Toward the development of an integrated biorefinery. Bioresour. Technol. 244, 328–337. https://doi.org/10.1016/j.biortech.2017.07.104
11. de Hoyos-Martínez, P.L., Erdocia, X., Charrier-El Bouhtoury, F., Prado, R., Labidi, J., 2018. Multistage treatment of almonds waste biomass: Characterization and assessment of the potential applications of raw material and products. Waste Manag. 80, 40–50. https://doi.org/10.1016/j.wasman.2018.08.051
12. Dragone, G., Kerssemakers, A.A.J., Driessen, J.L.S.P., Yamakawa, C.K., Brumano, L.P., Mussatto, S.I., 2020. Innovation and strategic orientations for the development of advanced biorefineries. Bioresour. Technol. 302, 122847. https://doi.org/10.1016/j.biortech.2020.122847
13. FAOSTAT, Food and Agriculture Organization of the United Nations. Crop statistics data. http://fao.org/faostat/en (accesed 10 April 2020).
14. Fernández-Rodríguez, J., Erdocia, X., Sánchez, C., González Alriols, M., Labidi, J., 2017. Lignin depolymerization for phenolic monomers production by sustainable processes. J. Energy Chem. 26, 622–631. https://doi.org/10.1016/j.jechem.2017.02.007
15. Gullón, B., Eibes, G., Dávila, I., Moreira, M.T., Labidi, J., Gullón, P., 2018. Hydrothermal treatment of chestnut shells (Castanea sativa) to produce oligosaccharides and antioxidant compounds. Carbohydr. Polym. 192, 75–83. https://doi.org/10.1016/j.carbpol.2018.03.051
16. Gullón, P., Eibes, G., Dávila, I., Moreira, M.T., Labidi, J., Gullón, B., 2018. Manufacture

of nutraceutical compounds from chestnut shells by hydrothermal processing. Chem. Eng. Trans. 70, 1705–1710. https://doi.org/10.3303/CET1870285
17. Hu, F., Jung, S., Ragauskas, A., 2013. Impact of pseudolignin versus dilute acid-pretreated lignin on enzymatic hydrolysis of cellulose. ACS Sustain. Chem. Eng. 1, 62–65. https://doi.org/10.1021/sc300032j
18. Huang, C., Lin, W., Lai, C., Li, X., Jin, Y., Yong, Q., 2019a. Coupling the post-extraction process to remove residual lignin and alter the recalcitrant structures for improving the enzymatic digestibility of acid-pretreated bamboo residues. Bioresour. Technol. 285, 121355. https://doi.org/10.1016/j.biortech.2019.121355
19. Huang, C., Wang, X., Liang, C., Jiang, X., Yang, G., Xu, J., Yong, Q., 2019b. A sustainable process for procuring biologically active fractions of high‐purity xylooligosaccharides and water‐soluble lignin from Moso bamboo prehydrolyzate. Biotechnol. Biofuels 12, 1–13. https://doi.org/10.1186/s13068-019-1527-3
20. Ioannidou, S.M., Pateraki, C., Ladakis, D., Papapostolou, H., Tsakona, M., Vlysidis, A., Kookos, I.K., Koutinas, A., 2020. Sustainable production of bio-based chemicals and polymers via integrated biomass refining and bioprocessing in a circular bioeconomy context. Bioresour. Technol 307, 123093. https://doi.org/10.1016/j.biortech.2020.123093
21. Kamelnia, E., Divsalar, A., Darroudi, M., Yaghmaei, P., Sadri, K., 2019. Industrial Crops & Products Production of new cellulose nanocrystals from Ferula gummosa and their use in medical applications via investigation of their biodistribution. Ind. Crop. Prod. 139, 111538. https://doi.org/10.1016/j.indcrop.2019.111538
22. Karimi, K., Taherzadeh, M.J., 2016. A critical review of analytical methods in pretreatment of lignocelluloses: Composition, imaging, and crystallinity. Bioresour. Technol. 200, 1008–1018. https://doi.org/10.1016/j.biortech.2015.11.022
23. Kasiri, N., Fathi, M., 2018. Production of cellulose nanocrystals from pistachio shells and their application for stabilizing Pickering emulsions. Int. J. Biol. Macromol. 106, 1023–1031. https://doi.org/10.1016/j.ijbiomac.2017.08.112
24. Kaur, M., Kumar, M., Sachdeva, S., Puri, S.K., 2020. An efficient multiphase bioprocess for enhancing the renewable energy production from almond shells. Energy Convers. Manag 203, 112235. https://doi.org/10.1016/j.enconman.2019.112235
25. Khili, F., Borges, J., Almeida, P.L., Boukherroub, R., Omrani, A.D., 2019. Extraction of Cellulose Nanocrystals with Structure I and II and Their Applications for Reduction of Graphene Oxide and Nanocomposite Elaboration. Waste and Biomass Valorization. 10 (7), 1913-1927. https://doi.org/10.1007/s12649-018-0202-4
26. Ko, C.H., Yang, B.Y., Lin, L.D., Chang, F.C., Chen, W.H., 2020. Impact of pretreatment methods on production of bioethanol and nanocrystalline cellulose. J. Clean. Prod. 254, 119914. https://doi.org/10.1016/j.jclepro.2019.119914
27. Liu, C., Hu, J., Zhang, H., Xiao, R., 2016. Thermal conversion of lignin to phenols: Relevance between chemical structure and pyrolysis behaviors. Fuel 182, 864–870. https://doi.org/10.1016/j.fuel.2016.05.104
28. Lizundia, E., Puglia, D., Nguyen, T., Armentano, I., 2020. Cellulose nanocrystal based multifunctional nanohybrids. Prog. Mater. Sci. 112, 100668. https://doi.org/10.1016/j.pmatsci.2020.100668
29. Ma, Z., Sun, Q., Ye, J., Yao, Q., Zhao, C., 2016. Study on the thermal degradation behaviors and kinetics of alkali lignin for production of phenolic-rich bio-oil using TGA-FTIR and Py-GC/MS. J. Anal. Appl. Pyrolysis 117, 116–124. https://doi.org/10.1016/j.jaap.2015.12.007

30. Morales, A., Gullón, B., Dávila, I., Eibes, G., Labidi, J., Gullón, P., 2018. Optimization of alkaline pretreatment for the co-production of biopolymer lignin and bioethanol from chestnut shells following a biorefinery approach. Ind. Crops Prod. 124, 582–592. https://doi.org/10.1016/j.indcrop.2018.08.032
31. Mujtaba, M., Salaberria, A.M., Andres, M.A., Kaya, M., Gunyakti, A., Labidi, J., 2017. Utilization of flax (Linum usitatissimum) cellulose nanocrystals as reinforcing material for chitosan films. Int. J. Biol. Macromol. 104, 944–952. https://doi.org/10.1016/j.ijbiomac.2017.06.127
32. Nabarlatz, D., Farriol, X., Montané, D., 2005. Autohydrolysis of almond shells for the production of xylo- oligosaccharides: Product characteristics and reaction kinetics. Ind. Eng. Chem. Res. 44, 7746–7755. https://doi.org/10.1021/ie050664n
33. Nitsos, C., Matsakas, L., Triantafyllidis, K., Rova, U., Christakopoulos, P., 2018. Investigation of different pretreatment methods of Mediterranean-type ecosystem agricultural residues: characterisation of pretreatment products, high-solids enzymatic hydrolysis and bioethanol production. Biofuels 9, 545–558. https://doi.org/10.1080/17597269.2017.1378988
34. Nitsos, C., Stoklosa, R., Karnaouri, A., Vörös, D., Lange, H., Hodge, D., Crestini, C., Rova, U., Christakopoulos, P., 2016. Isolation and Characterization of Organosolv and Alkaline Lignins from Hardwood and Softwood Biomass. ACS Sustain. Chem. Eng. 4, 5181–5193. https://doi.org/10.1021/acssuschemeng.6b01205
35. Orue, A., Eceiza, A., Arbelaiz, A., 2019. The use of alkali treated walnut shells as filler in plasticized poly(lactic acid) matrix composites. Ind. Crops Prod. 145, 111993. https://doi.org/10.1016/j.indcrop.2019.111993
36. Qiao, W., Li, S., Xu, F., 2016. Preparation and Characterization of a Phenol-formaldehyde Resin Adhesive Obtained from Bio-ethanol Production Residue. Polym. Polym. Compos. 24, 99–105. https://doi.org/10.1177/096739111602400203
37. Ruiz, H.A., Conrad, M., Sun, S.N., Sanchez, A., Rocha, G.J.M., Romaní, A., Castro, E., Torres, A., Rodríguez-Jasso, R.M., Andrade, L.P., Smirnova, I., Sun, R.C., Meyer, A.S., 2020. Engineering aspects of hydrothermal pretreatment: From batch to continuous operation, scale-up and pilot reactor under biorefinery concept. Bioresour. Technol. 299, 122685. https://doi.org/10.1016/j.biortech.2019.122685
38. Sequeiros, A., Gatto, D.A., Labidi, J., Serrano, L., 2014. Different extraction methods to obtain lignin from almond shell. J. Biobased Mater. Bioenergy 8, 370–376. https://doi.org/10.1166/jbmb.2014.1443
39. Sixta, H., 2006. Introduction. In: Sixta, H. (Ed.), Handbook of Pulp. WILEY-VCH Verlag GmbH &Co. KGaA., Weinheim, pp. 2-19. https://doi.org/10.1002/9783527619887
40. Sun, S.N., Li, M.F., Yuan, T.Q., Xu, F., Sun, R.C., 2012. Sequential extractions and structural characterization of lignin with ethanol and alkali from bamboo (Neosinocalamus affinis). Ind. Crops Prod. 37, 51–60. https://doi.org/10.1016/j.indcrop.2011.11.033
41. Tan, M., Ma, L., Rehman, M.S.U., Ahmed, M.A., Sajid, M., Xu, X., Sun, Y., Cui, P., Xu, J., 2019. Screening of acidic and alkaline pretreatments for walnut shell and corn stover biorefining using two way heterogeneity evaluation. Renew. Energy 132, 950–958. https://doi.org/10.1016/j.renene.2018.07.131
42. Thakur, M., Sharma, A., Ahlawat, V., Bhattacharya, M., Goswami, S., 2020. Process optimization for the production of cellulose nanocrystals from rice straw derived a -cellulose. Mater. Sci. Energy Technol. 3, 328–334. https://doi.org/10.1016/j.mset.2019.12.005
43. Urruzola, I., Robles, E., Serrano, L., Labidi, J., 2014. Nanopaper from almond (Prunus dulcis) shell. Cellulose 21, 1619–1629. https://doi.org/10.1007/s10570-014-0238-y
44. Wang, H., Xie, H., Du, H., Wang, X., Liu, W., Duan, Y., Zhang, Xiaoyi, Sun, L., Zhang,

Xinyu, Si, C., 2020. Highly Efficient Preparation of Functional and Thermostable Cellulose Nanocrystals via H2SO4 Intensified Acetic Acid Hydrolysis. Carbohydr. Polym. 239. 116233. https://doi.org/10.1016/j.carbpol.2020.116233

45. Wise, L.E., Maxine, M., D'Addieco, A.A., 1946. Chlorite holocellulose, its fractionation and bearing on summative wood analysis and on studies on the hemicelluloses. Tech. Assoc. pulp Pap. Ind. 29, 210-218.

46. Xiao, Y., Liu, Y., Wang, X., Li, M., Lei, H., Xu, H., 2019. Cellulose nanocrystals prepared from wheat bran: Characterization and cytotoxicity assessment. Int. J. Biol. Macromol. 140, 225–233. https://doi.org/10.1016/j.ijbiomac.2019.08.160

47. Xu, C., Liu, F., Alam, M.A., Chen, H., Zhang, Y., Liang, C., Xu, H., Huang, S., Xu, J., Wang, Z., 2020. Comparative study on the properties of lignin isolated from different pretreated sugarcane bagasse and its inhibitory effects on enzymatic hydrolysis. Int. J. Biol. Macromol. 146, 132–140. https://doi.org/10.1016/j.ijbiomac.2019.12.270

48. Zang, G., Shah, A., Wan, C., 2020. Techno-economic analysis of an integrated biorefinery strategy based on one-pot biomass fractionation and furfural production. J. Clean. Prod. 260, 120837. https://doi.org/10.1016/j.jclepro.2020.120837

49. Zhang, J., Deng, H., Sun, Y., Pan, C., Liu, S., 2010. Isolation and characterization of wheat straw lignin with a formic acid process. Bioresour. Technol. 101, 2311–2316. https://doi.org/10.1016/j.biortech.2009.11.037

50. Zhu, L., O'Dwyer, J.P., Chang, V.S., Granda, C.B., Holtzapple, M.T., 2008. Structural features affecting biomass enzymatic digestibility. Bioresour. Technol. 99, 3817–3828. https://doi.org/10.1016/j.biortech.2007.07.033

Figure list

Figure 1. Flowchart of the integral biorefinery scheme developed for the overall valorisation of almond shells.

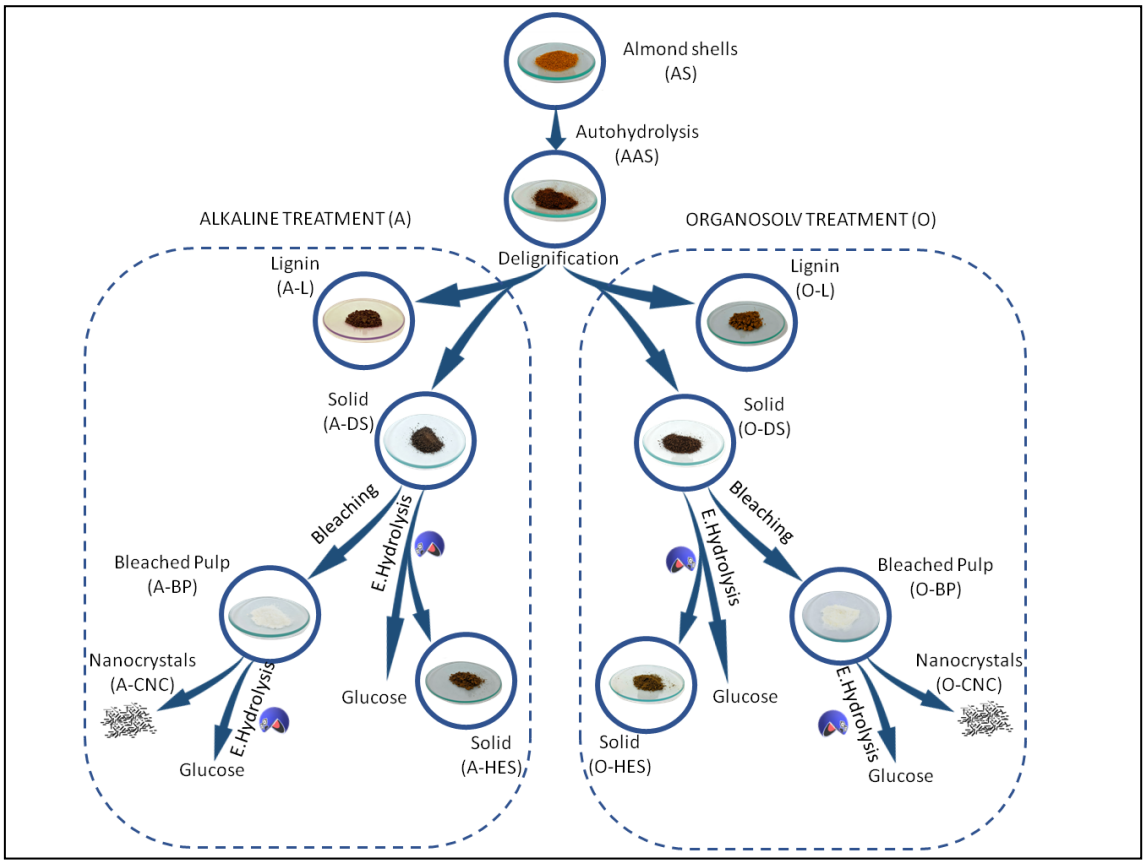

Figure 2. Glucan to glucose conversion during the enzymatic hydrolysis of differently pretreated Almond Shells.

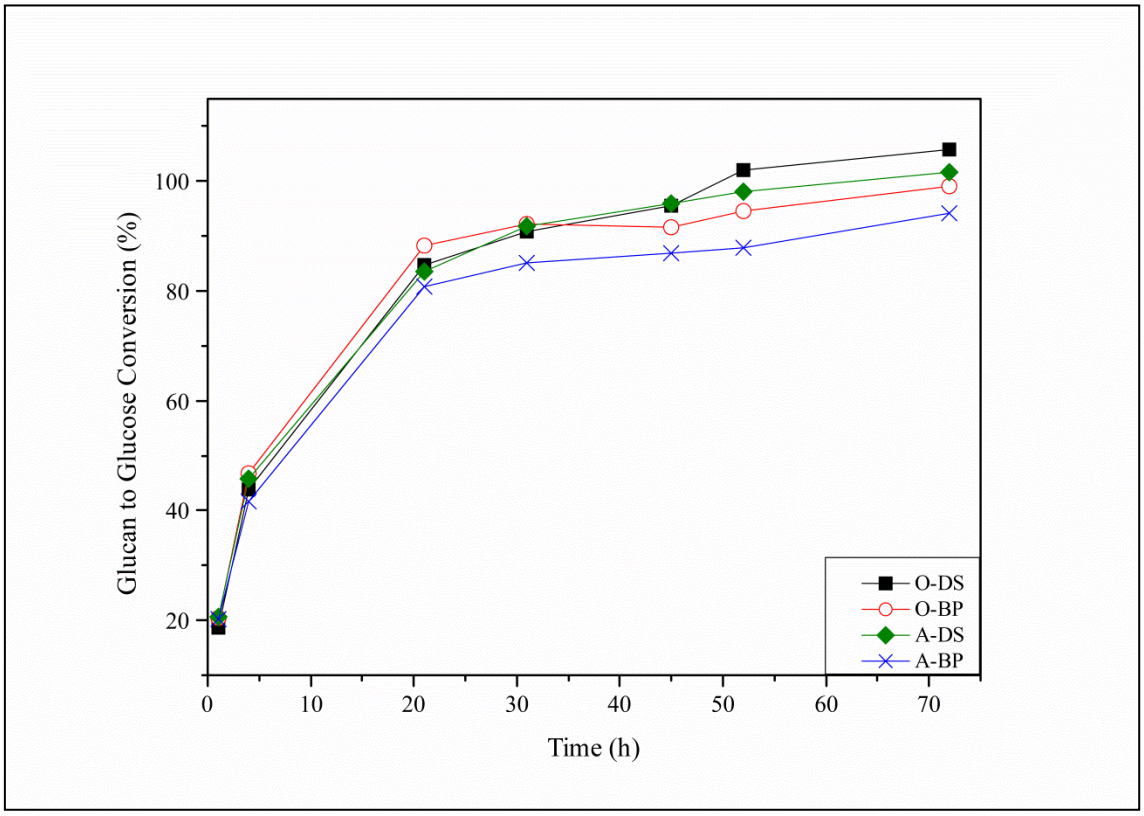

Figure 3. TGA and DTG curves for Almond Shells (AS), Autohydrolysis Solid (AAS), Delignified Solids (O-DS and A-DS), post-Enzymatic Hydrolysis Solids (O-HES and A-HES), Bleached Pulps (O-BP and A-BP) and Cellulose Nanocrystals (O-CNC and A-CNC) after organosolv [a and c] and alkaline [b and d] processing.

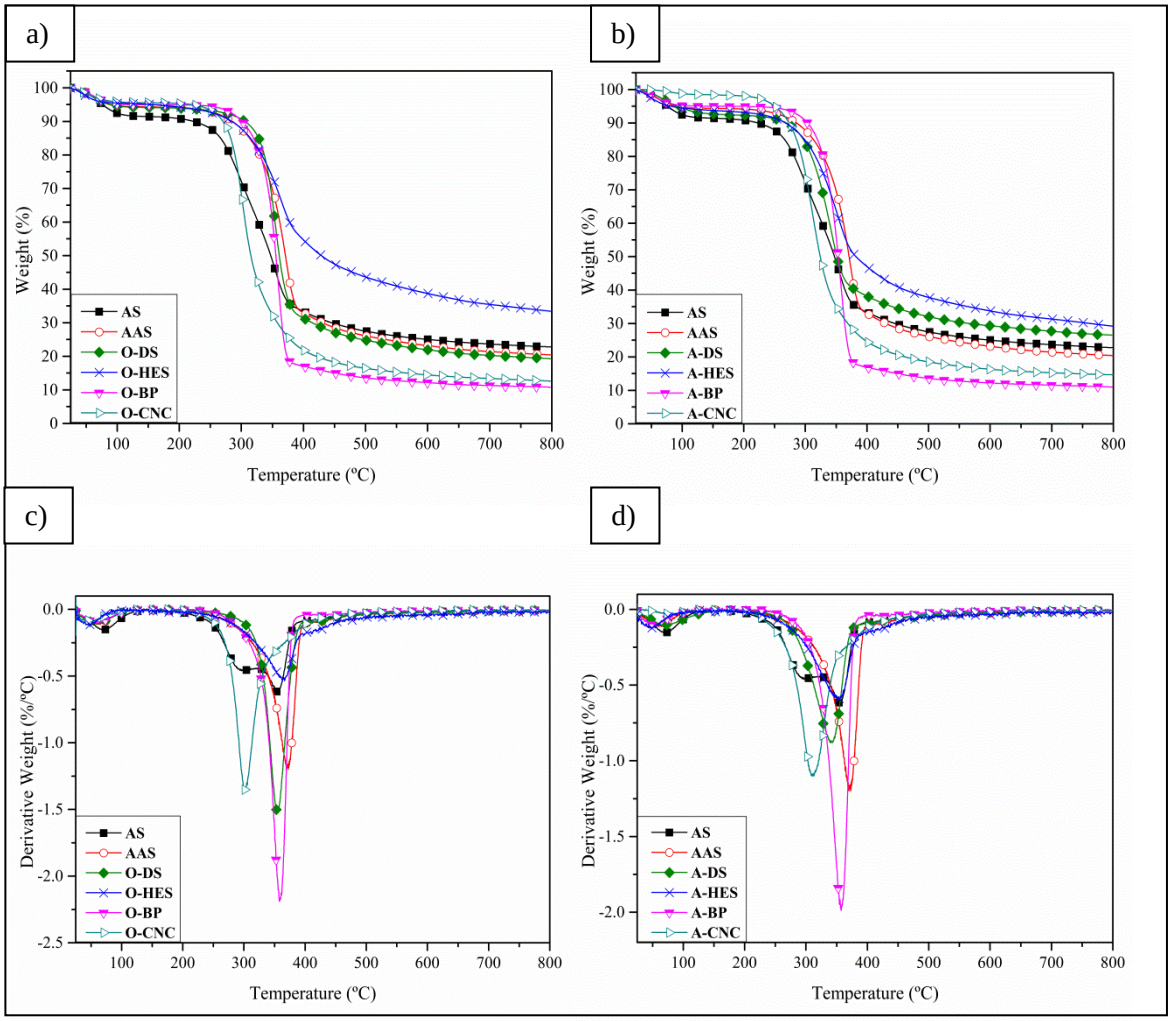

Figure 4. AFM images and profile of the height values along the sample in the marked area of 2D AFM images of a) O-CNC b) A-CNC.

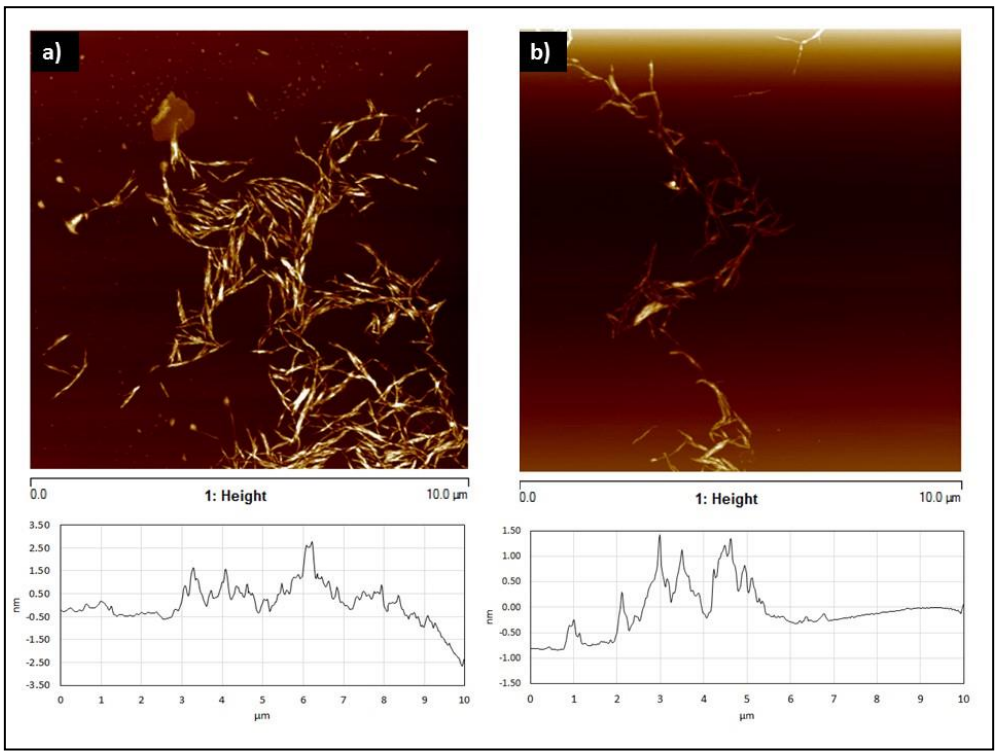

Figure 5. TGA and DTG curves for organosolv lignin (O-L) and alkaline lignin (A-L).

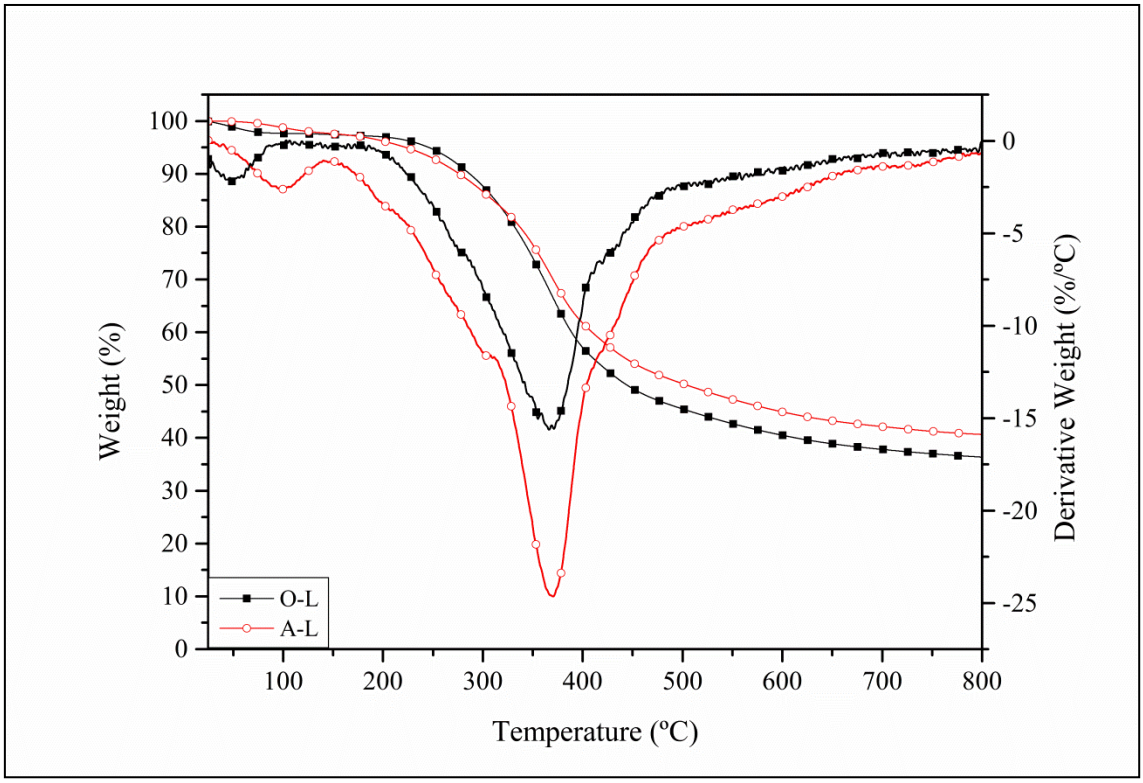

Table 1. Methods employed for the characterisation of raw material, solid and liquid fractions.

Analysis	Sample	Equipment	Reference
Chemical characterisation of the raw material			
Moisture Ash Extractive content	AS		TAPPI T264-om-88 TAPPI T211-om-02 TAPPI T204-cm-97
Hemicelluloses, glucan and lignin content	AS	HPLC-RI/PDA (Jasco LC-Net II/ADC, 300 × 7.8 mm Aminex HPX-87H column)	NREL-TP-510-42618 (Dávila et al., 2017)
Analysis of the solids obtained after different treatments			
Moisture	AAS, O-DS, A-DS, O-BP, A-BP, O-HES and A-HES		TAPPI T264-om-88
Chemical characterisation	AAS, O-DS, A-DS, O-BP, A-BP, O-HES and A-HES	HPLC-RI/PDA (Jasco LC-Net II/ADC, 300 × 7.8 mm Aminex HPX-87H column)	NREL-TP-510-42618 (Dávila et al., 2017)
Chemical characterisation of the liquid phase from autohydrolysis treatment			
Quantification of the monosaccharides and acetic acid	Liquid phase from autohydrolysis and post-hydrolysis	HPLC-RI/PDA (Jasco LC-Net II/ADC, 300 × 7.8 mm Aminex HPX-87H column)	(Dávila et al., 2017)
Non-volatile compound	Liquid phase from autohydrolysis		(Dávila et al., 2017)
Characterisation of the lignin			
Purity	O-L and A-L	HPLC-RI/PDA (Jasco LC-Net II/ADC, 300 × 7.8 mm Aminex HPX-87H column)	(Dávila et al., 2017)
Total phenolic content	O-L and A-L	UV-Vis spectrophotometer (Jasco V-630, JASCO)	(Morales et al., 2018)
Average molecular weight, number-average and polydispersity index	O-L and A-L	GPC (JASCO LC-Netll/ADC, detector: RI-2031Plus, Two PolarGel-M columns: 300 mm x 7.5 mm)	(Morales et al., 2018)

Composition	O-L and A-L	Py-GC/MS (Py: 5150 Pyroprobe, GC: Agilent 6890, MS: Agilent 5973)	(Dávila et al., 2017)
Structural and chemical characterisation			
Chemical structure	AS, AAS, O-DS, A-DS, O-BP, A-BP, O-HES, A-HES, O-L and A-L	ATR-FTIR (PerkinElmer Spectrum Two FTIR Spectrometer)	(Dávila et al., 2019)
Crystallinity	AS, AAS O-DS, A-DS, O-BP, A-BP, O-HES, A-HES, O-CNC and A-CNC	XRD (Phillips X'Pert Pro Automatic multipurpose diffractometer)	(Karimi and Taherzadeh, 2016; Thakur et al., 2020; Xiao et al., 2019)
Thermogravimetric analysis	AS, AAS, O-DS, A-DS, O-BP, A-BP, O-HES, A-HES, O-L and A-L	TGA/DTG (TGA/SDTA RSI analyser 851 Mettler Toledo)	(Mujtaba et al., 2017)
Surface morphology and size of the nanocrystals	O-CNC and A-CNC	AFM (Dimension 3100 NanoScope IV, Veeco)	(Mujtaba et al., 2017)

GPC: gel permeation chromatography, Py-GC/MS: Pyrolysis-Gas Chromatography/Mass Spectrometry, ATR-FTIR: Attenuated Total Reflectance - Fourier Transformed Infrared Spectroscopy, XRD: X-Ray Diffraction, TGA: Thermogravimetric Analysis, AFM: Atomic Force Microscopy.

Table 2. Composition of the solids after autohydrolysis, delignification, bleaching and enzymatic hydrolysis.

	Composition (wt.%)			Loss during the Treatment (wt.%)		
Treatment	**Lignin**	**Glucan**	**Hemicelluloses**	**Lignin**	**Glucan**	**Hemicelluloses**
AAS	38.98	31.26	11.12	24.77	0	80.19
O-DS	38.41	46.32	10.11	35.09	2.39	40.11
A-DS	34.66	50.38	6.45	37.12	0	59.77
O-BP	0	63.23	16.87	100	2.21	0
A-BP	0	75.06	10.15	100	1.15	0
O-HES	76.11	8.22	0	56.00	96.07	100
A-HES	78.08	4.39	0	27.40	97.19	100

Table 3. Identification of the Py-GC/MS products from O-L and A-L samples.

	Organosolv		**Alkaline**		**Origin***
Compound	**R.T. (min)**	**Area (%)**	**R.T. (min)**	**Area (%)**	
Furfural	-	-	5.039	0.76	C
o,m,p-cresol	8.630-9.047	1.25	8.630-9.047	1.16	P
Guaiacol	9.330	6.43	9.382	8.48	G
Homoguaiacol	11.409	8.23	11.490	10.30	G
Catechol	11.507	1.14	11.594	1.90	S
3-Methoxycatechol	11.344	5.03	13.453	6.66	S
4-Ethylguaiacol	13.846	3.06	13.962	4.84	G
4-Methylcatechol	-	-	14.412	1.25	S
4-Vinylguaiacol	15.019	4.52	15.076	3.27	G
Syringol	16.093	9.14	16.226	13.23	S
Eugenol	16.202	1.43	-		G
3,4-dimethoxyphenol	16.301	2.23	16.422	3.31	S
Vanillin	17.248	2.40	17.358	1.53	G
cis-Isoeugenol	17.375	1.33	-		G
4-Methylsyringol	18.241	14.37	18.305	13.97	S
4-Ethylsyringol	19.610	2.08	19.668	3.84	S
Vinylsyringol	20.239	3.11	20.274	1.83	S
Methoxyeugenol	20.794	1.51	-	-	G
4-Allylsyringol	21.475-22.134	4.70	-	-	S
Hexadecanoic acid, methyl ester	24.571	1.24	-	-	FA
Palmitic acid	24.958	3.42	-	-	FA
Octadecanoic acid, methyl ester	26.650	1.24	-	-	FA
Stearic acid	-	-	26.933	3.10	FA
Total S compounds	41.80		45.99		
Total G compounds	28.91		28.42		
Ratio S/G	1.45		1.62		

*C: carbohydrate; P: phenol; G: guaiacol; S: syringol; FA: fatty acids